Health Monitoring of High Strain Composites Using Embedded Fiber Bragg Grating Sensors

Brayden Aller* and Sergio Pellegrino†
California Institute of Technology, Pasadena, CA, 91125

Nathan Kinkaid‡, Juan Mejia-Ariza§, and Richard Otis¶
Jet Propulsion Laboratory (JPL), California Institute of Technology, Pasadena, CA, 91109

Patrick Hon Man Chan‖ and Francisco Pena**
NASA Armstrong Flight Research Center (AFRC), Edwards, CA, 93523

A study on the use of fiber Bragg grating sensors to measure strains in thin-walled composite structures is presented. It includes measurement of the gage factor, or strain conversion coefficient, of small diameter fiber optic sensors. Fiber Bragg grating sensor arrays were embedded into high strain composites and the buildup of strains during manufacturing was tracked. μCT scans of these composites were taken after curing to analyze the micro-structure in the regions surrounding the embedded sensors. Composite laminates with embedded sensors were subjected to a controlled coiling experiment to evaluate the accuracy of the sensors in measuring internal strains.

I. Introduction

High strain composites (HSC) are of great interest in the development of future spacecraft structures due to their low areal density and ability to be elastically packaged with high efficiency. Two current efforts investigating the use of such structures are the NASA Advanced Composite Solar Sail System (ACS3), which is an upcoming flight project that will demonstrate NASA's deployable composite boom technology [1], and the Caltech Space Solar Power Project which plans to use thin composite Triangular Rollable And Collapsible (TRAC) longerons as primary structural elements in creation of solar power satellites up to 60 m × 60 m in size [2].

Large spacecraft structures based on HSC are packaged and stowed for a period of time before their deployment in space. During this time, the structures are kept in a high strain state that can lead to degradation in the performance of the structure due to micro-structural changes or the propagation of damage within the structure. The cause of these effects is still an active area of research [3], and particularly in the packaged configuration, it is important to have a way to be able to detect and measure such changes in the structure throughout its lifetime. To most effectively track these changes, the key parameter of interest to measure is the strain within the structures. While there are many sensing systems capable of taking these measurements, fiber Bragg grating (FBG) sensors are especially well-suited as they are small, lightweight, flexible, and capable of high spatial resolution distributed sensing. FBG sensors are a type of optical fiber sensor in which gratings, or regions of locally higher refractive indices, are inscribed into the core of an optical fiber [4]. The basic principle of FBG sensors is that when a spectrum of light shines down the optical fiber all of the wavelengths are transmitted through except for a particular wavelength known as the Bragg wavelength, λ_B, which is proportional to both the spacing between gratings, Λ, and the effective refractive index of the optical fiber, n_e, via [5]:

$$\lambda_B = 2n_e\Lambda \tag{1}$$

As these parameters change in response to an applied strain or temperature, a resulting shift in λ_B will occur. This shift

*Graduate Student, Graduate Aerospace Laboratories, 1200 E California Blvd, MC 105-50, AIAA Student Member. baller@caltech.edu

†Joyce and Kent Kresa Professor of Aerospace and Civil Engineering, Graduate Aerospace Laboratories, 1200 E California Blvd, MC 105-50, AIAA Fellow. sergiop@caltech.edu

‡Mechanical Engineer, Spacecraft Mechanical Engineering, 4800 Oak Grove Dr.

§Technologist; Materials Development, Testing and Failure Investigations Group, 4800 Oak Grove Dr., AIAA Senior Member

¶Technologist, Materials Development and Manufacturing Technology, 4800 Oak Grove Dr.

‖Electronics Engineer, Advanced Systems Development Branch, P.O. Box 273, Edwards, California

**Aerospace Engineer, Aerostructures Branch, P.O. Box 273, Edwards, California, AIAA Member

can then be measured and converted into either a temperature or strain measurement, according to the relationship

$$\frac{\Delta\lambda_B}{\lambda_{B,0}} = \alpha\varepsilon + \beta\Delta T \tag{2}$$

where $\Delta\lambda_B$ is the measured shift in the Bragg wavelength, $\lambda_{B,0}$ is the original Bragg wavelength for the FBG, α is the gage factor, ε is the strain of the fiber, β is the thermo-optic coefficient, and ΔT is the change in temperature.

FBG-based sensors have the ability to take thousands of distributed point strain measurements along a single optical fiber [6] and have been used for a wide variety of aerospace applications ranging from the shape sensing of aircraft wings [7] to measuring strains in large composite cylinders as a part of NASA's Shell Buckling Knockdown Factor (SBKF) Project [8].

The goal of the present work is to develop an in-situ monitoring system using this technology that will give both the ability to monitor the health of large composite space structures from manufacturing to end-of-life, and the opportunity to better understand how these structures behave and change under a wide variety of conditions.

II. Embedded Sensor Placement

There are several ways in which FBG sensors can be embedded into thin composite laminates. When choosing where to embed the sensor within the laminate there are two primary considerations. The first is the alignment of the fiber optic sensor with the surrounding carbon fibers. When the sensor is not embedded parallel to the surrounding carbon fibers, resin pockets, or locally resin-rich regions in the laminate, can form and reduce the strength of the laminate. The weakening introduced by the misalignment of the FBGs with the surrounding carbon fibers has been shown in [9] with thicker laminates and this effect would become more pronounced in the thin laminates of interest in this work.

The second primary consideration is determining the location of interest for measurement within the laminate. Depending on where the sensor is located in the laminate the measured strains by the sensor will vary. In Fig. 1, there are three examples of different sensor placements within thin symmetric, cross-ply laminates, each of which would measure different strains if the laminate is loaded in bending. In Fig. 1a, the sensor is located within the outer ply of the laminate enabling it to measure strains in the laminate introduced by bending since it is away from the mid-surface. In Fig. 1b, the sensor is placed such that the core of the optical fiber, where the FBG is located, is at the outer surface of the laminate. In the context of bending, this will enable the measurement of either the largest tensile or compressive strains observed by the laminate. And finally in Fig. 1c, the FBG sensor is attached to the outer surface of the laminate with a structural adhesive. This approach enables the measurement of the strains on the outer surface of the laminate without having to embed the sensor directly within the laminate, but would prevent the tight packaging of the structure.

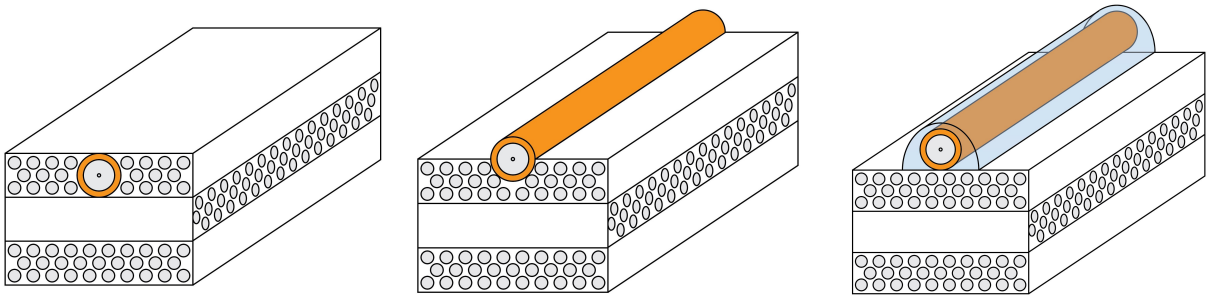

(a) In outer ply **(b) Halfway in outer ply** **(c) Surface mounted**

Fig. 1 Possible FBG sensor placement in thin laminate.

III. Implementation

The ultimate goal of this work is to develop a monitoring scheme to track the condition of thin composite structures from manufacturing to end-of-life through a variety of conditions using a network of embedded FBG sensors. As preliminary work towards the development of this scheme, studies on several key aspects of health monitoring using

FBG sensors have been conducted. These areas of study will be briefly introduced here and the specific work that has been done is presented in the following sections.

A. Sensor Calibration and Baseline Measurements

Before any measurements can be taken, the FBG sensors must first be calibrated to find their sensitivity to both strain and/or temperature depending on specific testing parameters. This corresponds to finding the values of α and/or β respectively in Eq. 2.

The basic principle of sensing with FBGs is to convert a relative shift in the reflected wavelength from a known reference value to either a temperature or strain measurement. Therefore, a baseline value of the reflected wavelength $\lambda_{B,0}$ must be obtained for each FBG. This is done by measuring the reflected wavelength of each sensor in a reference configuration from which either strains or changes in temperature will be measured.

B. Cure Monitoring

The first step in the life cycle of thin composite space structures is the manufacturing process. In this approach, the strain is measured throughout the layup process to track initial strains on the FBG introduced during this process and to monitor for any damage to the sensor that may affect its measurements. Measurements are also taken before and after curing the composite laminate, to track the buildup of residual strains along the embedded FBGs during this process.

C. Experiments

To evaluate the ability of the sensors to measure the strains within thin, high strain composites and to detect changes in HSC structures throughout their lifetime, it is important to conduct controlled experiments that simulate conditions that may be experienced by the structures. One such condition is the coiling of HSC structures. Coiling is a common form of packaging as it enables a high packing efficiency. During this process, the structures are held in a high strain state that can lead to changes in the structure over time, making it of interest for testing. To do this, a controlled coiling experiment will be conducted in which test coupons with embedded FBG sensors are coiled around a hub of known size. Strain measurements are taken while these coupons are held in this configuration to evaluate the accuracy of embedded FBG sensors to measure strains during coiling.

IV. Determination of Gage Factor

To accurately convert the measured shifts in wavelength to strain, the value of the gage factor α for the FBG sensors must be determined. A standard value for the gage factor of optical fibers is $\alpha = 0.78$ [10]. As a check to determine if this value is accurate for the small diameter FBG sensors used in this study, a sensor calibration study was conducted.

In this test, individual FBG sensors were mounted into an Instron load frame and subjected to repeated tensile loading cycles. During each cycle, the strain experienced by the FBG was precisely measured with a vertical extensometer that recorded the small changes in the distance between the two pieces of retro reflective tape located on either side of the FBG region of the optical fiber. In parallel with the strain measurements, the corresponding wavelength shifts of the FBG, $\Delta\lambda_B$, were recorded using a FBG interrogator. Eqn. 2 was then used to solve for α assuming $\Delta T = 0$ since this testing was conducted in a temperature-controlled laboratory environment. This testing was conducted with four different FBG sensors each with a different starting center wavelength (1530 nm, 1540 nm, 1550 nm and 1560 nm) and each undergoing 10 loading and unloading cycles. For each loading and unloading of the FBG, an average value of α was calculated, leading to a total of 20 measurements for each of the four FBGs. The results of these calibration measurements can be seen in Fig. 2a along with the testing setup in Fig. 2b. With the exception of the 1540 nm FBG, the average values of α obtained for the rest of the FBGs were close to this assumed value of $\alpha = 0.78$ and therefore this value will be used to calculate the measurements of strain in this paper. However, it is noted that there were sizable deviations in the measured values of α for all four FBGs tested and the cause of this spread will be investigated further in future work.

V. Curing of High Strain Composites with Embedded FBGs

For the remaining studies, two thin composite plates with embedded FBG sensors were manufactured. These plates were constructed out of nine plies of 30 grams per square meter (gsm) unidirectional carbon fiber prepreg with T800 carbon fibers and NTPT ThinPreg 402 epoxy resin with a layup of [0_3/90_3/0_3 with FBGs], where the FBG sensor array

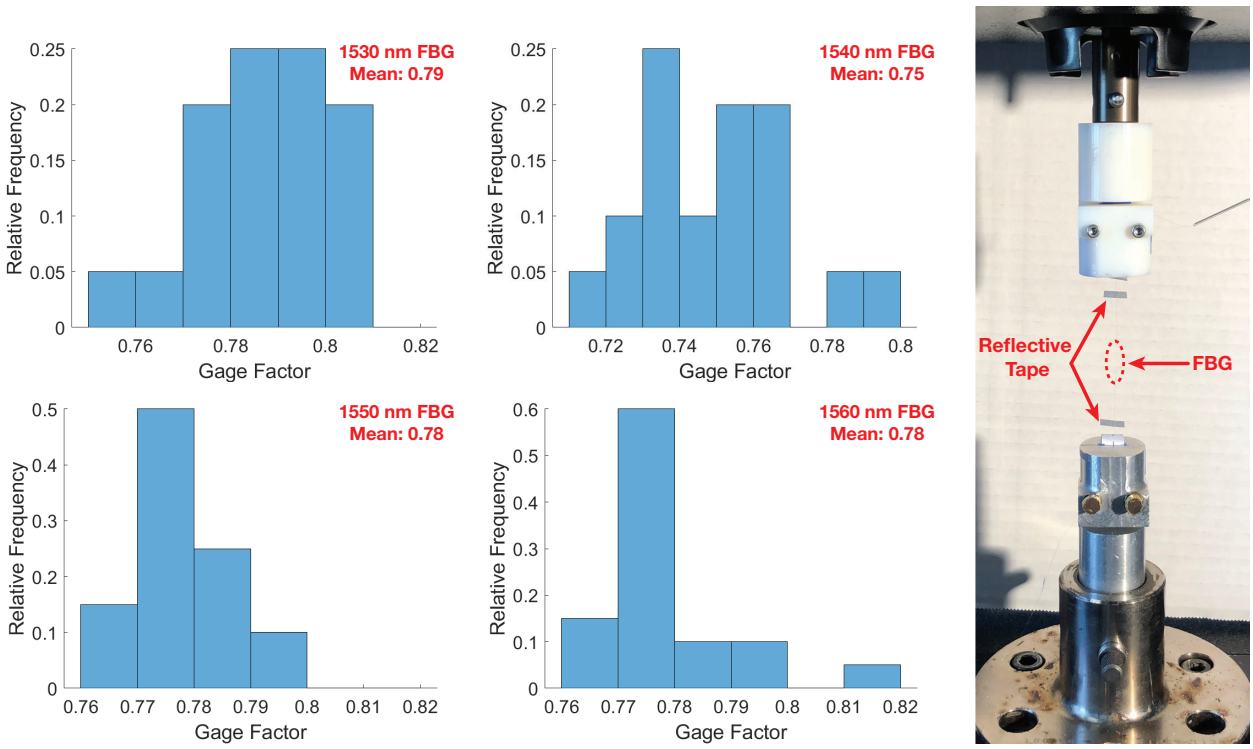

(a) Calibration results **(b) Test setup**

Fig. 2 Calibration of FBGs.

is embedded in the bottom three plies. This construction, similar to that depicted in Fig. 1a, was chosen to offset the FBG sensor array from the mid-surface of the plate to measure coiling strains. Additionally, it was chosen to construct these samples out of nine plies so the layer of three 0° plies in which the fiber was embedded was at least as thick as the embedded FBG array to ensure good relative alignment with the surrounding carbon fibers, while remaining a simple cross-ply laminate. To help protect the optical fiber ingress/egress regions of the laminate, a thin polymer buffer region was incorporated into the ends of the laminate. The fiber ingress/egress points into the laminate are the most common point of failure of FBG sensors embedded into composite parts [4]. This is due to the large stiffness mismatch between the laminate and the optical fiber at these points. This buffer consists of two thin polymer films bonded together around the fiber and acts to provide strain relief for the optical fiber by reducing the stiffness mismatch between the laminate and the embedded fiber. This buffer tapers down in width after exiting the laminate to provide a gradual reduction in stiffness. A picture of one of the test coupons after curing can be seen in Fig. 3 with the approximate FBG locations marked.

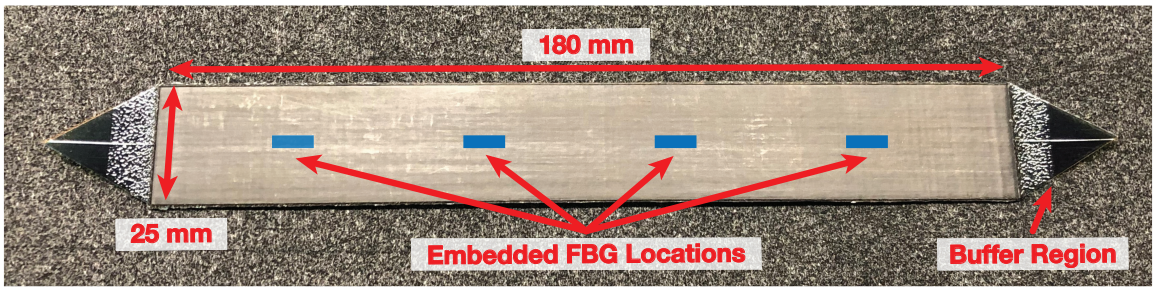

Fig. 3 Test coupon with embedded FBG array.

The FBG arrays embedded in these plates consisted of Fibercore's SM1500(4.2/50)P optical fiber which has a nominal coated diameter of 71 μm, a protective polyimide coating, and a temperature rating higher than 200°C, making

them ideally suited for embedment in thin composites. Each array has four FBG sensors with a center-to-center spacing of 40 mm. These gratings are each capable of measuring strain ranges of ± 8000 $\mu\varepsilon$, which exceeds the expected strains in this work.

During the layup and curing of each of these samples, FBG measurements were taken at key points in the process to track the build-up of strains experienced by the FBG. These were collected after the fiber was embedded in the bottom three 0° plies, after the middle three 90° plies were added, after the top three 0° plies were added, and after the curing process. These measurements were collected with a Luna HYPERION si255 FBG interrogator at ambient temperature. A buildup of strains observed by the FBGs in each coupon can be seen in Fig. 4.

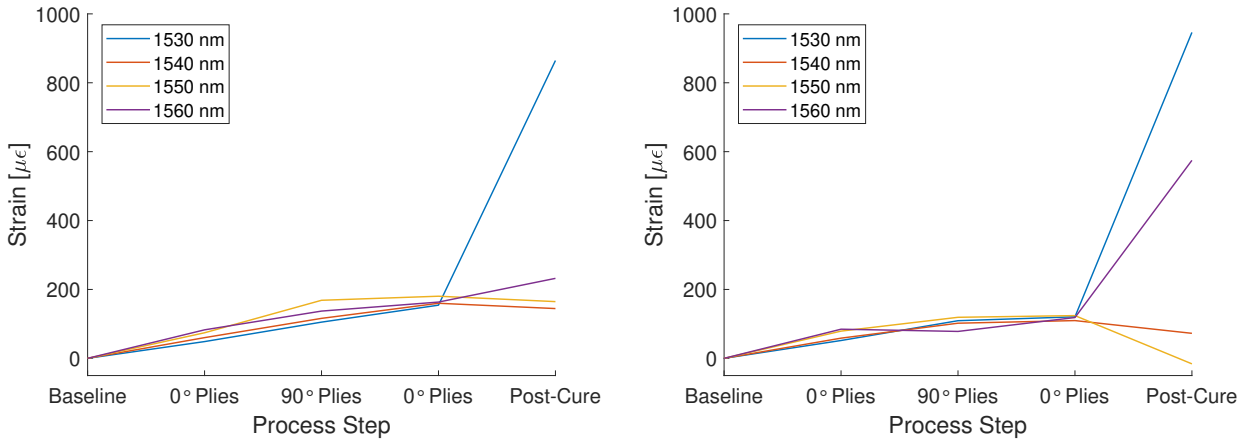

(a) Coupon 1 **(b) Coupon 2**

Fig. 4 Strain buildup in test coupons during manufacturing process.

In these plots, it can be seen that the buildup of strains along the embedded FBGs was fairly uniform between the individual FBG sensors during the layup process. However, after curing it can be seen that the strains in the different FBG sensors on the coupons varied widely. To identify possible causes for the large disparity in residual strains observed, μCT scans were taken at several FBG locations. These were taken with a ZEISS Xradia 510 Versa 3D X-ray microscope with an approximate resolution of 1 μm. The three locations of interest identified for closer analysis are the 1530 nm FBG in Coupon 1, the 1560 nm FBG in Coupon 1, and the 1550 nm FBG in Coupon 2. These three locations were chosen to explore the microstructure of the laminate in regions where the residual strain increased significantly during curing (1530 nm FBG in Coupon 1), increased by a small amount (1560 nm FBG in Coupon 1), and became compressive (1550 nm FBG in Coupon 2). Cross-sectional images taken from each of the three scans are presented in Figs. 5-7.

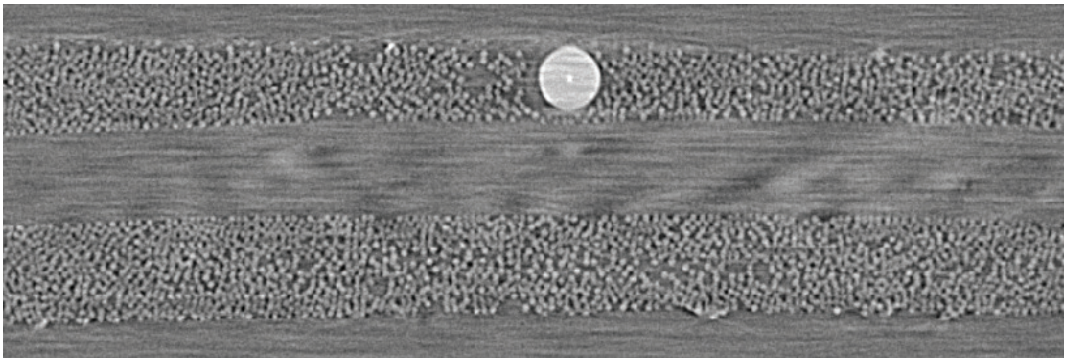

Fig. 5 Cross-section of 1530 nm FBG in Coupon 1.

Looking at Figs. 5-7, we can see that the micro-structure of the laminate is different in these three regions, which could play a part in explaining the difference in the observed strains in these three areas. In Fig. 5, it can be seen that there appears to be good fiber consolidation around the optical fiber with some small resin-rich regions to the left.

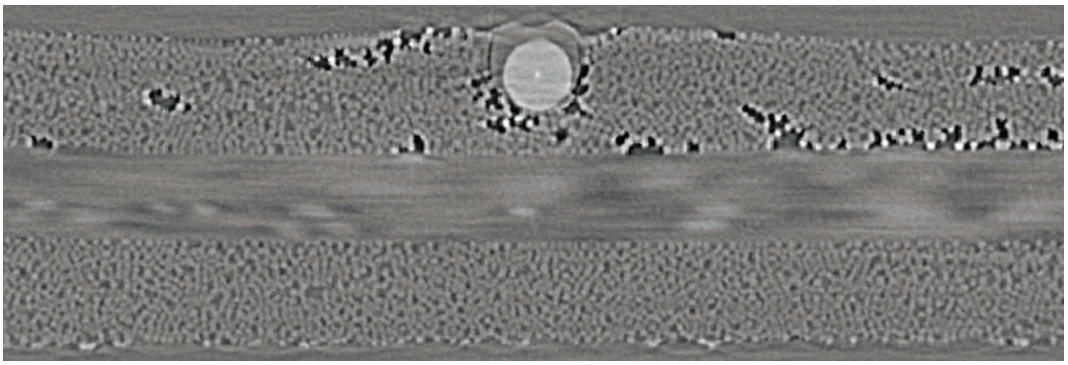

Fig. 6 Cross-section of 1560 nm FBG in Coupon 1.

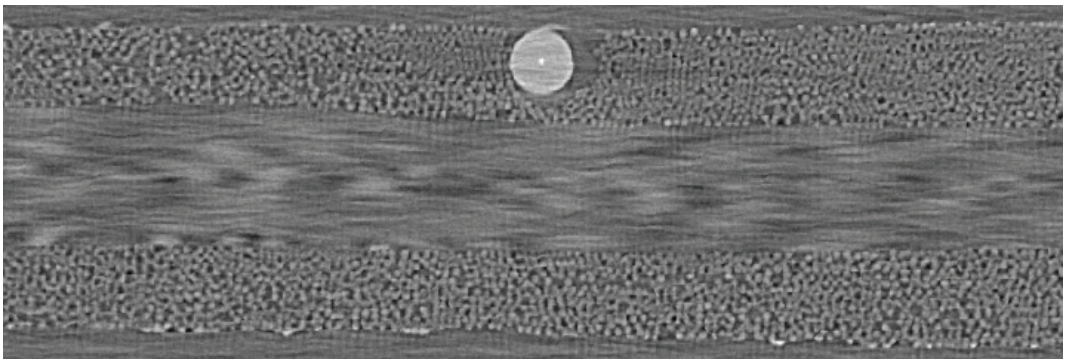

Fig. 7 Cross-section of 1550 nm FBG in Coupon 2.

Additionally, it can be seen that the layer of fibers the optical fiber is embedded in is thinner than the other two layers of the laminate with some variance in thickness across the width of the image. In Fig. 6, it can be seen that at this location there are voids surrounding the optical fiber throughout the layer of 0° fibers in which it is embedded and that this layer is thicker than the other two layers with its thickest point being at the location of the fiber. Also, the polyimide coating on the fiber, which is the darker region that surrounds the fiber, is not concentric with the fiber. In Fig. 7, it can be seen that the fibers directly around the fiber and to the right are more closely packed than in the rest of the laminate. Here, we can also see variations in thickness of the three layers and non-concentricity of the fiber coating with most of its thickness located to the right of the fiber. Future work will be conducted to investigate how each of these micro-structural features affects the residual strain buildup along the embedded optical fibers.

VI. Coiling of High Strain Composites with Embedded FBGs

To test the ability of embedded FBG sensors to measure the strains within HSC in a configuration of interest, the two test coupons discussed in Section V were coiled around a 100 mm diameter hub using an in-house developed coiling machine. This machine co-coils the coupons with a thin Kapton membrane that applies a uniform normal pressure on the surface of the coupons to enable tight coiling. Images of a test coupon being coiled using this machine can be seen in Fig 8.

The samples were coiled such that the embedded FBG sensors were located on the side furthest from the hub, resulting in a tensile strain at the sensor location. Measurements were taken from these coupons while they were held in the coiled configuration using the Luna HYPERION si255 interrogator, and the strain changes were computed using the wavelength readings from the cured test coupons in a flat configuration as baseline $\lambda_{B,0}$ values. It is noted that the membrane tension when coiling the coupons directly affects the amount of applied pressure

$$P = \frac{T}{R_h w_m} \tag{3}$$

where T is the membrane tension, R_h is the hub radius and w_m is the width of the membrane. These tests were

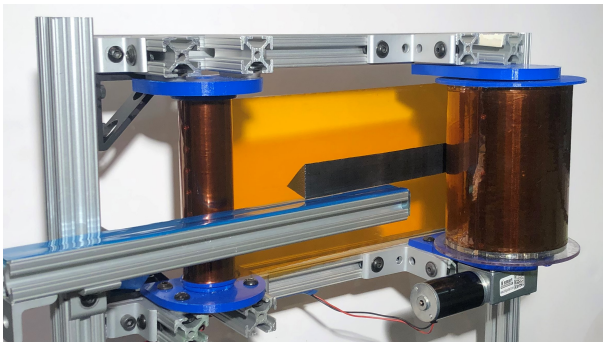

(a) Uncoiled configuration

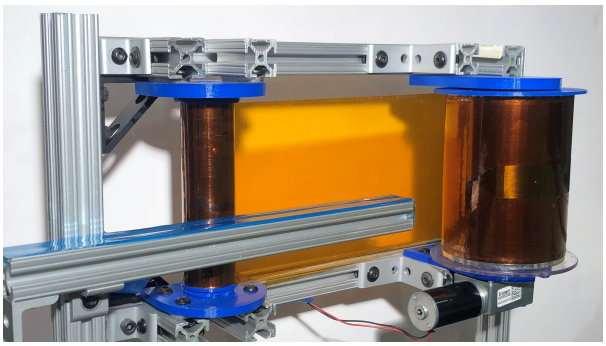

(b) Coiled configuration

Fig. 8 Coiling of a test coupon.

conducted at three different membrane tensions of approximately 5 N, 9.5 N and 14 N to observe if the pressure exerted by the membrane on the sample had any effect on the strains recorded. These correspond to membrane pressures of approximately 0.8 kPa, 1.5 kPa and 2.2 kPa respectively. Each test was repeated twice for both coupons. The strains measurements are provided in Table 1 for Coupon 1 and Table 2 for Coupon 2.

Table 1 Coupon 1 coiling strains ($\mu\varepsilon$)

	1530 nm		1540 nm		1550 nm		1560 nm	
	Test 1	Test 2	Test 1	Test 2	Test 1	Test 2	Test 1	Test 2
5 N	1950	1916	1773	1811	1680	1692	1728	1623
9.5 N	1935	1928	1770	1854	1673	1689	1731	1676
14 N	1894	1902	1765	1883	1661	1681	1727	1650

Table 2 Coupon 2 coiling strains ($\mu\varepsilon$)

	1530 nm		1540 nm		1550 nm		1560 nm	
	Test 1	Test 2	Test 1	Test 2	Test 1	Test 2	Test 1	Test 2
5 N	1741	1736	1557	1575	1626	1603	1738	1821
9.5 N	1736	1741	1567	1583	1615	1617	1855	1835
14 N	1713	1722	1578	1573	1601	1613	1843	1833

From these results, two key observations can be made. First, the strains readings from the individual FBGs during this testing varied from around 1550 to 1950 $\mu\varepsilon$. One possible explanation for this spread is thickness variations of the laminates as seen in Figs. 5-7. Since the applied membrane pressures were rather small, most of the strain experienced by the embedded FBGs in this coiling experiment can be attributed to bending.

Considering the simple bending formula

$$\varepsilon = \kappa z \tag{4}$$

where ε is the strain observed at distance z above the mid-plane of a plate subject to an imposed curvature κ, a rough estimate of how much the observed strain at the FBG location varies with changes in thickness of the laminate can be obtained. A radius of curvature of 50.1 mm (= $1/\kappa$) and a distance z = 0.1 mm approximate the experimental conditions and laminate geometry. Perturbing these values slightly, it can be seen that ε is insensitive to changes in the radius of curvature, varying only ± 4 $\mu\varepsilon$ with a change of ∓ 0.1 mm, which would correspond to very large changes in laminate thickness. On the other hand, if z is perturbed by ± 1 μm, the change in predicted ε is ± 20 $\mu\varepsilon$. This indicates that small changes in the thickness of the laminate that shift the position of the embedded fiber can potentially have a significant effect on the observed strain value. The second key observation was the observed strains didn't generally appear to

be significantly affected by the changes in membrane pressure applied to the coupons. This is as expected since the pressures applied were very small.

During this testing, it was also noticed that several spectral peaks from which the FBG peak wavelength values are extracted began to broaden and showed smaller side peaks. Examples of some of these effects are shown, alongside their baseline spectral profile when the embedded sample is in the flat configuration, in Figs. 9 and 10.

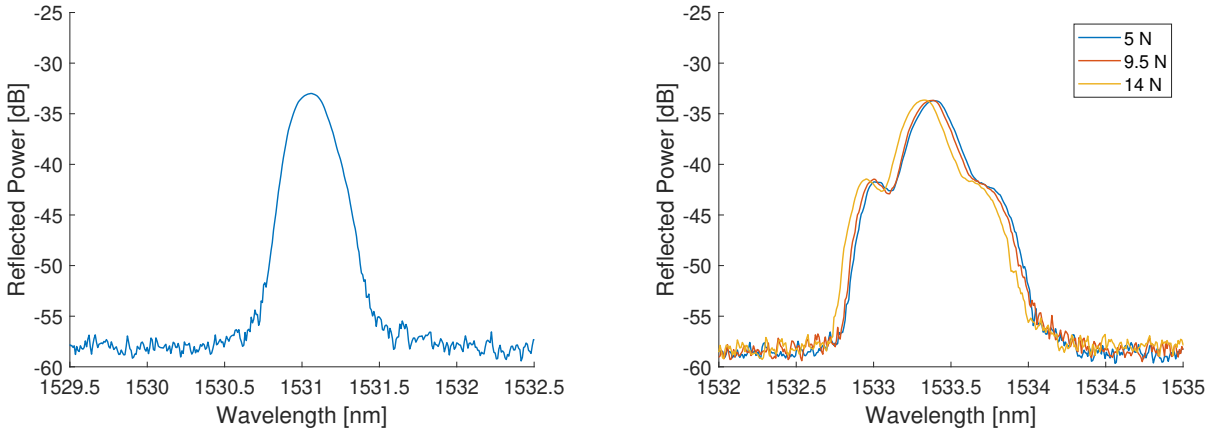

(a) Flat configuration spectral peak **(b) Coiled configuration spectral peak**

Fig. 9 Spectral variation of 1530 nm FBG in Coupon 1.

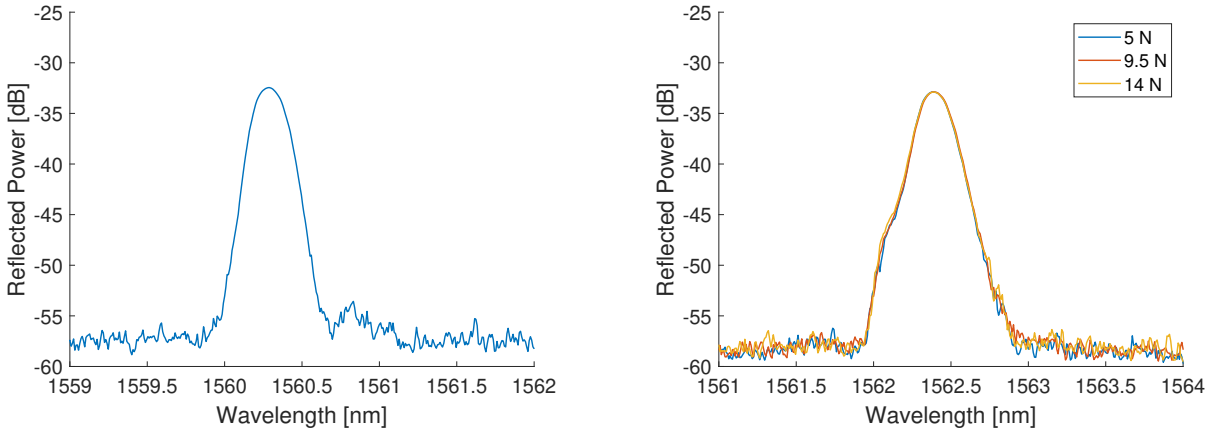

(a) Flat configuration spectral peak **(b) Coiled configuration spectral peak**

Fig. 10 Spectral variation of 1560 nm FBG in Coupon 1.

In both Figs. 9 and 10 it can be seen that the spectral peaks in the flat configuration are narrow and have clear peaks. However, in both of these examples the spectra became distorted when the coupon is in the coiled configuration. In Fig. 9b, the peak widens significantly and a small side peak forms on the left. In Fig. 10b, we can see that the peak has widened and is slightly distorted on the left. It can also be seen in Figs. 9b and 10b that the distorted spectral profiles of the FBGs didn't vary with the membrane tension. In these tests, these distortions didn't hinder our ability to measure the wavelength of the primary peak and get a strain reading, but if these effects were to become more prominent, it could negatively affect our ability to be able to accurately measure the strains observed by the FBG. Therefore, the underlying causes of these distortions will be investigated in future work.

VII. Conclusions

In this work, preliminary studies towards the development of a health monitoring system of HSC structures using embedded FBG sensors has been conducted. The first study measured the gage factor α of small-diameter FBG arrays. While most of the results were aligned with the standard value of $\alpha = 0.78$, there was a wide spread of results. Further testing and analysis will need to be conducted to understand this distribution and more accurately determine the gage factor of these arrays. In the second study, FBG arrays were successfully embedded into thin HSC laminates. During the manufacturing and curing process, measurements were taken to track the buildup of strains on the embedded FBGs. It was observed that the buildup of strains during the layup process was fairly uniform for all FBGs in a coupon, but there were wide variations in the recorded strains after the curing process. μCT scans were taken at several FBG locations to determine possible causes of these differences. These scans revealed a variety of micro-structural defects ranging from voids around the FBG to local variations in ply thickness around the FBG. Further investigation will need to be conducted to understand how changes in the composite micro-structure affect the residual strains observed by the embedded FBGs. The final study was a coiling experiment where test coupons with embedded FBG sensors were co-coiled around a hub with a thin Kapton membrane and the strains observed during coiling were measured for various membrane tensions. Large variations in the measured strains were found between the individual FBGs, but the changes in strain due to varying membrane pressure were small. Distortions of the FBG spectra during coiling were observed. These distortions were not found to change significantly with changes in membrane pressure. Further study is needed to understand the underlying causes of these spectral distortions.

Acknowledgments

The research was carried out in part at the Jet Propulsion Laboratory, California Institute of Technology, under a contract with the National Aeronautics and Space Administration (80NM0018D0004). The authors would like to acknowledge the contributions of Antonio Pedivellano, Charles Sommer, Alan Truong and Alexander Wen in the design and construction of the coiling machine used in this work and for their assistance in its operation.

References

[1] Wilkie, W. K., Fernandez, J. M., Stohlman, O. R., Schneider, N. R., Dean, G. D., Kang, J. H., Warren, J. E., Cook, S. M., Brown, P. L., Denkins, T. C., Horner, S. D., Tapio, E. D., Straubel, M., Richter, M., and Heiligers, J., "An Overview of the NASA Advanced Composite Solar Sail (ACS3) Technology Demonstration Project," *AIAA SciTech Forum*, 2021. https://doi.org/10.2514/6.2021-1260.

[2] Gdoutos, E. E., Truong, A., Pedivellano, A., Royer, F., and Pellegrino, S., "Ultralight Deployable Space Structure Prototype," *AIAA SciTech Forum*, 2020. https://doi.org/10.2514/6.2020-0692.

[3] Ubamanyu, K., Hasanyan, A. D., and S, P., "Experimental Study of Time-dependent Failure of High Strain Composites," *AIAA SciTech Forum*, 2020. https://doi.org/10.2514/6.2020-0207.

[4] Udd, E., and Spillman Jr, W. B., *Fiber Optic Sensors*, 2nd ed., Wiley, Hoboken, 2011, Chap. 15.

[5] Richards, W. L., Parker, A. R., Ko, W. L., Piazza, A., and Chan, P., "Application of Fiber Optic Instrumentation," NATO RTO-AG-160, 2012.

[6] Chan, P., "Fiber Optic Sensing System (FOSS) at NASA Armstrong Flight Research Center (AFRC): Summary and Recent Deployments," NASA AFRC-E-DAA-TN60829, 2018.

[7] Pena, F., "Fiber-Optic Strain-Based Deflection and Twist Sensing for a High-Aspect-Ratio Swept Wing," NASA/TM-2020-220465, 2020.

[8] Pena, F., Richards, W. L., Parker, A. R., Piazza, A., Schultz, M. R., Rudd, M. T., Gardner, N. W., and Hilburger, M. W., "Implementation of Fiber Optic Sensing System on Sandwich Composite Cylinder Buckling Test," *AIAA SciTech Forum*, 2018. https://doi.org/10.2514/6.2018-1695.

[9] Shivakumar, K., and Emmanwori, L., "Mechanics of Failure of Composite Laminates with an Embedded Fiber Optic Sensor," *Journal of Composite Materials*, Vol. 38, No. 8, 2004, pp. 669, 680. https://doi.org/10.1177/0021998304042393.

[10] Kashyap, R., *Fiber Bragg Gratings*, 2nd ed., Academic Press, Burlington, 2010, Chap. 10.